International Journal of Modern Developments in Engineering and Science
Volume 2, Issue 12, December 2023
https://www.ijmdes.com | ISSN (Online): 2583-3138


# Dynamic Modeling of Fixed-bed Column Adsorption of Methylene Blue onto Modified Kono-Bowe (Nigerian) Clay

Ajemba Regina Obiageli[1], Nweke Chinenyenwa Nkeiruka[2*], John Sunday Uzochukwu[3]
[1,2,3]*Department of Chemical Engineering, Nnamdi Azikiwe University, Awka, Anambra, Nigeria*

***Abstract*: Dynamic modeling of fixed-bed column adsorption of methylene blue onto modified Kono-bowe clay was studied. The modified clay sorbent was characterized. The effect of initial concentration, flow rate and bed height on the adsorption process was investigated. Three kinetic models, Thomas, Adams-Bohart, and Yoon-Nelson, were applied to the experimental data to predict the breakthrough curves. Also, the bed depth service time (BDST) model was employed to predict the time needed for breakthrough at other process conditions. Results of the adsorbent characterization show that the modification process altered the structure of the natural clay. Experimental data confirmed that the breakthrough curves were dependent on the initial concentration, flow rate and bed height. The Thomas and Yoon-Nelson models fitted very well to the experimental data. The experimental data were in good agreement with the BDST model. This study showed that modified Kono-bowe clay column can be used to treat wastewater.**

***Keywords*: breakthrough curve, clay adsorbent, dynamic modelling, fixed-bed adsorption, methylene blue.**

## 1. Introduction

Water pollution has become so rampant in our society as a result of proliferation of industries. Most of these industries make use of colouring pigments like dyes and discharge their effluents untreated into rivers, streams, lakes, etc. Dyes are widely used in many fields of advanced technology, e.g., cosmetics, printing, pharmaceutical, textile, paint, leather tanning, paper, food processing [1]-[7], etc. Dyes are toxic and carcinogenic and their discharge into the water possess a source of significant pollution that leads to reduction in sunlight penetration, retards photosynthetic activity, inhibits the growth of biota [8]-[11]. Among the numerous available dyes, methylene blue finds wider application in industrial processes, which include paper colouring, coating for paper stock, dyeing cotton, wools, etc. Acute exposure to Methylene blue may cause increased heart rate, shock, vomiting, cyanosis, jaundice, quadriplegia, Heinz body formation and tissue necrosis in humans [12].

The removal of color from industrial dye-bearing effluents has posed a major problem due to their non-biodegradability and difficulty in treating such wastewaters by conventional treatment methods. Such conventional treatment techniques include; chemical coagulation/flocculation, ion-exchange [13], ultra-filtration, membrane separation, reverse osmosis [14], advanced oxidation [15], [16] and adsorption [7], [17]-[26] etc. Among these conventional treatments, adsorption is considered to be the most economical and requires less area and is not sensitive to either diurnal variation or to toxic chemicals [27]. Among the adsorbents studied, attention has been drawn to natural materials capable of removing pollutants from contaminated waters and at the same time low in cost. Many researchers have tested different adsorbents efficiency such as activated carbon [28]-[30], clay minerals [31]-[33], zeolite [34], silica [35], chitin [36], [37] and coal [38] for lowering the dye concentration in wastewater. Clay minerals have been indicated as an amply suitable alternative [39].

Clays are environmental friendly, cheaply available with high cation exchange capacity, surface area, chemical and mechanical stability, Bronsted and Lewis acidity [40]. These special clay properties can be enhanced by treatment of the clays with concentrated inorganic acids such as hydrochloric acid, sulfuric acid, phosphoric acid, nitric acid, etc. Present investigations have shown that acid activation of clays followed by thermal treatment has further increased these properties to a greater extent [41]. Acid activation of clay minerals replaces the exchangeable cations in both the tetrahedral and octahedral sites with $H^+$ ions accompanied by the release of $Al^{3+}$, while leaving the $SiO_4$ groups largely intact [42], [43]. Such treatment leads to transformation of the clay crystalline structure to amorphous metakaolin and the octahedral Al ions are preferentially released from the clay structure leading to formation of additional Al-OH and Si-OH bonds, without troubling the original mineral structure [44]-[47].

Most studies on treatment of wastewater containing methylene blue dye by adsorbents have been performed in batch experiments and only a few have been reported in fixed-bed column systems which are more relevant to real operating systems on natural waters. Both batch adsorption and fixed-bed adsorption studies are required to obtain key parameters required for the design of fixed-bed adsorber. Batch adsorption studies are performed to obtain the key parameters such as isotherm constants and pore diffusivity, while fixed-bed

*Corresponding author: cn.nweke@unizik.edu.ng

adsorption is used to determine the experimental breakthrough curve [48].

In this present study, acid/thermal activated Kono-bowe clay has been used to evaluate its effectiveness in methylene blue adsorption by determining adsorption capacity parameters, kinetics and adsorption. The main target of the present study is to find out the important design parameters such as depth of exchange zone, adsorption rate, and adsorption capacity of a fixed-bed column for methylene blue–clay adsorption system. The breakthrough curves for the adsorption of MB dye were also analyzed by using the well-known mathematical models such as Thomas, Yoon-Nelson, and Adams-Bohart models.

## 2. Materials and Methods

### *A. Preparation of methylene blue solution*

The Methylene blue used in this work was purchased from Conraws Chemical Company in Enugu. Stock solution was prepared by dissolving 1.0 g of MB in 1 L of distilled water without further purification. The test solutions of Methylene blue were prepared by diluting the stock solution with distilled water to the desired concentration. The pH of each solution was adjusted to the required value with diluted hydrochloric acid and sodium hydroxide during the experiment.

### *B. Activation of the clay adsorbent*

Clay from Kono-bowe (N: 8° 32' 05"; E: 8° 55' 05"; A: 126m) River state of Nigeria was mined from the site and sun-dried for 72 hours. The dried clay sample was sieved with a local basket to remove large impurities, and then ground to small particles by the aid of mortar and pestle. The acid activation was done by the procedure outlined by [49]. 30 g of clay was mixed with 300 mL of 1 M $H_2SO_4$ for 3 h. the slurry formed was filtered via a Buchner funnel and the residue washed with distilled water severally until it was free from sulphate ion and then dried at 383 K in an air oven until constant weight was obtained. The acid-activated clay sample was then thermally activated in a muffle furnace at 450 $^0$C for 2 h. The acid/thermal activated sample was ground to the required size and used in the adsorption experiment.

### *C. Characterization of the adsorbent*

The activated clay adsorbent used in this study was characterized with scanning electron microscopy (SEM), x-ray diffraction (XRD), x-ray fluorescence (XRF), surface area (SA) using Sears' method [50] and cation exchange capacity (CEC) according to Bergaya and Vayer (51) as reported in Sarma et al., [43]. To measure the cation exchange capacity of the adsorbent, 50 mL of 1 M $CuCl_2$ solution was mixed with 102 ml of 1 M ethylene-di-amine solution. The mixture was diluted with distilled water to 1 L to give a 0.05 M solution of the formed complex. 0.5 g of dry activated clay sample was mixed with 5 mL of the complex solution in a 100 mL flask, diluted with distilled water to 25 mL, and the mixture was agitated for 30 min in a thermostatic water bath shaker and centrifuged. The concentration of the complex remaining in the supernatant was determined by mixing 5 mL of it with 5 mL of 0.1 M HCl to destroy the complex, followed by the addition of 0.5 b KI per mL and then titrating Cu (II) iodometrically with 0.02 M $Na_2S_2O_3$ in the presence of starch as indicator. The CEC was calculated from the following formula:

$$CEC\ \left(\frac{meg}{100g}\right) = MSV\frac{x-y}{1000m} \quad (1)$$

Where $M$ = molar mass of the complex, $S$ = strength of the thio solution, $V$ = volume (mL) of the complex taken for iodometric titration, $m$ = mass of adsorbent taken (g), $x$ = volume (ml) of thio required for blank titration (without the adsorbent), $y$ = volume (ml) of thio required for the titration (with the adsorbent).

To measure the surface area by Sears' method [50], 0.5 g of clay was acidified with 0.1 HCl to pH of 3 to 3.5. After adding 10 g of NaCl, the volume was made up to 50 mL with distilled water and titrated with standard 0.1 N NaOH (temperature adjusted to 303 K) slowly till the pH was 4.0, and the titration was carried out till the pH reached a steady value of 9.0. The volume, V, required for raising the pH from 4.0 to 9.0 was noted and the surface area was estimated from the equation:

$$S\ \left(\frac{m^2}{g}\right) = 32\,V - 25 \quad (2)$$

### *D. Column adsorption studies*

For continuous adsorption experiments in a fixed-bed column, studies were conducted in a glass column with internal diameter of 1.5 cm and a height of 30 cm, packed with a known quantity of clay adsorbent. A known concentration of MB solution was pumped in down flow mode at desired flow rates using a peristaltic pump. At the exit of the column, samples were collected at regular intervals of 60 min to determine its MB concentration. The effects of the following column parameters on MB adsorption were investigated. (i) Effect of bed height: bed height was varied between 2.0 cm (0.7 g), 5 cm (0.90 g), 7 cm (1.12 g) and 9 cm (1.50 g), keeping flow rate and initial MB concentration constant at 0.6 L/min and 50 mg/L, respectively. (ii) Effect of flow rate: flow rate was varied between 0.15 L/min, 0.3 L/min, 0.6 L/min and 0.9 L/min, while bed height and inlet MB concentration were held constant at 5 cm and 50 mg/L, respectively. (iii) Effect of inlet MB concentration was varied between 20 mg/L, 50 mg/L, 80 mg/L and 120 mg/L, at 5 cm bed height and 0.6 L/min flow rate.

### *E. Evaluation of basic adsorption column design parameters*

The performance of a fixed-bed adsorption column can be described through the concept of breakthrough curve (BTC).

Table 1
X-ray fluorescence analysis of the clay samples [Ajemba, 2014]

| Clay samples | Chemical constituents | | | | | | | | | |
|---|---|---|---|---|---|---|---|---|---|---|
| | $Al_2O_3$ | $SiO_3$ | $Fe_2O_3$ | MgO | $Na_2O$ | $K_2O$ | CaO | $TiO_2$ | LOI | Total |
| Natural | 25.78 | 52.65 | 10.94 | 1.73 | 0.96 | 0.61 | 1.13 | 2.41 | 4.79 | 100 |
| Modified | 2.63 | 89.59 | 1.71 | 0.92 | 0.01 | 0.05 | 0.08 | 1.28 | 3.34 | 99.61 |

The time for breakthrough, $t_b$, and the shape of the breakthrough curve are very important parameters for determining the operations and dynamics of an adsorption column. The experimental data was analyzed to determine the design parameters of breakthrough curves for packed bed column. The fixed-bed capacity, that is total dye adsorbed, $q_{total}$ (mg), is equal to the area under the plot of the adsorbed MB concentration $C_{ad}$ (mg/L) versus time (min) and is calculated as follows;

$$q_{total} = \frac{QA}{1000} = \frac{Q}{1000} \int_{t=0}^{t=total} C_{ad}\ dt \quad (3)$$

Where $C_{ad} = C_o - C_t$; $Q$ and $A$ are the flow rate (L/min) and area under the breakthrough curve, respectively, $C_o$ (mg/L) is the initial MB concentration and $C_t$ (mg/L) is the MB concentration at time, $t$.

The total MB uptake capacity ($q_{exp}$, mg/g) of the fixed-bed column is calculated by dividing the total amount of MB adsorbed by the mass of the adsorbent (g) packed inside the column as given in equation 4;

$$q_{exp} = \frac{q_{total}}{m} \quad (4)$$

Total amount of MB sent to the fixed-bed column ($m_{total}$) can be evaluated from equation (5):

$$m_{total} = \frac{C_o Q t_{total}}{1000} \quad (5)$$

where $t_{total}$ is the total flow time.

The total percentage removal of MB, that is, the column performance can be determined by the following equation,

$$Total\ MB\ removal, R(\%) = \frac{q_{total}}{m_{total}}\ x\ 100 \quad (6)$$

The effluent volume ($V_{eff}$) was calculated from equation (7) as,

$$V_{eff} = Q t_{total} \quad (7)$$

where $t_{total}$ is the total flow time.

To characterize the breakthrough curve (BTC), the mass transfer zone (MTZ) model is used. This involves the mass transfer zone height, velocity, and time.

The time required for the mass transfer zone to move the length of its own height up/down the column once it has become established is,

$$t_z = \frac{V_E - V_B}{Q} = t_E - t_B \quad (8)$$

Where, $V_E$ is the total volume of effluent treated to the point of exhaustion (L); $V_B$ is the total volume of effluent treated to the point of breakthrough (L); $t_B$ is the breakthrough time.

The time required for the mass transfer zone to become established and move completely out of the bed is,

$$t_E = \frac{V_E}{Q} \quad (9)$$

The rate at which the mass transfer zone is moving up or down through the bed is,

$$U_z = \frac{h_z}{t_z} = \frac{h}{t_E - t_f} = \frac{h}{t_{st}} \quad (10)$$

Where, $h_z$ is the height of mass transfer zone (cm); $h$ is the total bed height (cm); $t_f$ is the time required for the mass transfer zone to initially form (min); $t_{st}$ is the stoichiometric time (time at which $C/C_o = 0.5$).

The length of the mass transfer zone is given by the expression;

$$h_z = U_z t_z = h\left(\frac{t_z}{t_E - t_f}\right) = h\left(\frac{t_E - t_B}{t_E}\right) \quad (11)$$

## 3. Results and Discussions

### *A. A. Characterization of the clay adsorbent*

#### *1) Surface area (SA)*

Activation of clay by acid treatment and subsequent calcination has been shown to be effective in limiting possible decomposition of the crystalline structure and in increasing the specific surface area [41]. The acid treatment opens up the edges of the platelets and as a consequence, the surface area and the pore diameter increase [52]. These conclusions are in conformity with the results obtained in this work. The surface area of the natural clay was measured to be 27.43 $m^2/g$, but increased to a value of 89.74 $m^2/g$ after modification by acid activation and subsequent calcination at 450 $^{\circ}C$.

#### *2) Cation exchange capacity (CEC)*

The CEC of the clay adsorbent was measured as outlined in the experimental section. The CEC value of the activated clay sorbent was observed to increase over that of natural clay. The value of the CEC of the natural clay was recorded as 18.4 meq/100 g, but after activation (acid and subsequent thermal), the CEC increased to 49.8 meq/100 g. The increase in CEC after activation could be attributed to the replacement of large number of different cations with $H^+$ ions and on subsequent heating/calcination, to a higher temperature, 450 $^0C$, resulted to the loss of the inter lamellar water and de-hydro-oxylation of the alumino-silicate lattice. This de-hydro-oxylation results to increase in the Lewis acidity at the expense of the Bronsted acidity [52]. The ion exchange capacity of clay minerals is attributed to structural defects, broken bonds, and structural hydroxyl transfers [53].

#### *3) Scanning electron microscopy (SEM)*

The raw and acid/thermally modified Kono-bowe clay samples were examined under scanning electron microscopy (SEM) to investigate the morphological and surface characteristics and the images are shown in Figures 1 and 2. The leaching of cations from the clay surface by acid activation created voids on the clay thereby making the clay surface more porous. As the acid activated sample was further subjected to thermal activation (Figure 2) clumps of uneven surface can be

seen along with some flat flakes of low porosity, which rendered the clay surface rather flat.

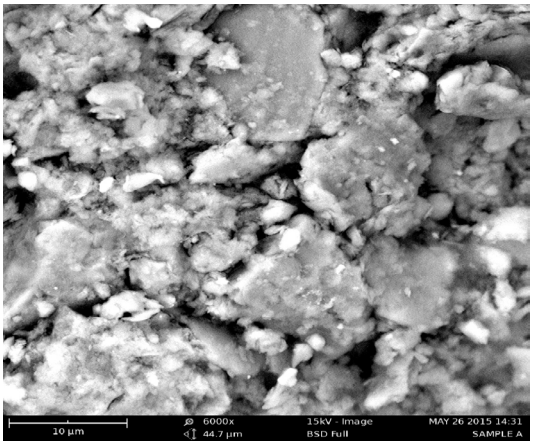


Fig. 1. Scanning electron microscope (SEM) images of natural clay

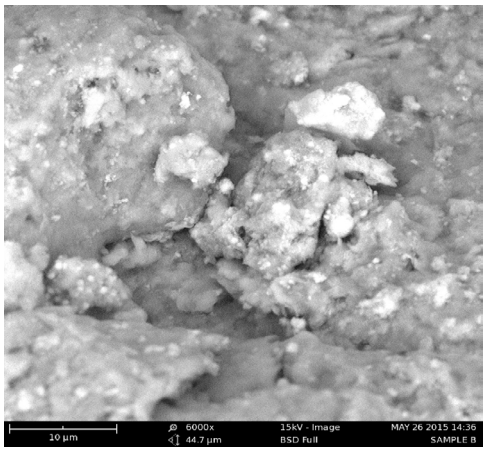


Fig. 2. Scanning electron microscope (SEM) images of modified clay

### *4) X-ray diffraction (XRD) [Ajemba, 2014]*

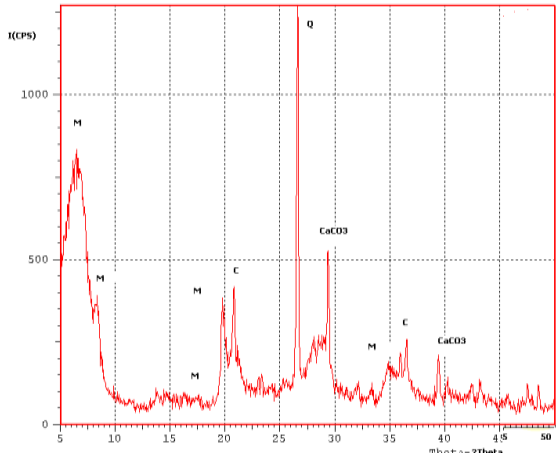


Fig. 3. XRD patterns for the natural clay adsorbent [Ajemba, 2014]

The XRD patterns of raw and acid/thermal activated Kono-bowe clay are shown in Figures 3 and 4, respectively. Montmorillonite (M) was the main mineral; however, minor amounts of quartz (Q), chrystoballitte (C) and calcium carbonate are present and these results are in accordance with literature publications [54]-[56]. The strong diffraction peaks at $2\theta$ = 26.7° and 31.06° can be ascribed to the characteristic diffraction of quartz and chrystoballite impurities [57], respectively, which indicated the existence of quartz impurities. Also, the diffraction peaks at $2\theta$ =21.6° and 36.4° reveal the presence of small amounts of calcites. After acid/thermal treatment, the characteristic peaks of montmorillonite, calcium carbonate, and chrystoballite almost disappeared, indicating that these impurities were removed. The diffraction peaks at $2\theta$ = 7.45° are assigned to the (110) characteristic peaks of sepiolites [58], [59].

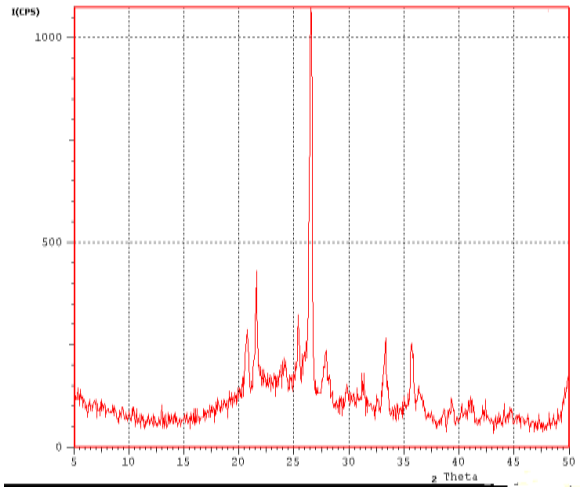


Fig. 4. XRD patterns for the modified clay adsorbent [Ajemba, 2014]

### *5) XRF analysis results of the clay mineral*

X-ray fluorescence spectrophotometer was employed in the analysis of the chemical composition of natural and acid/thermal activated samples. The results of the analysis are presented in Table 1 [41]. From the table, it can be seen that the chemical composition of the natural Kono-bowe clay is mainly composed of silica ($SiO_2$), alumina ($Al_2O_3$) and iron oxide ($Fe_2O_3$), with traces of calcium, sodium, potassium, magnesium, and titanium oxides in form of impurities. The decrease of the content of calcium, magnesium, sodium, and potassium oxides in the clay minerals after treatment with the acid and subsequent calcination at 450 $^0$C shows that metal cations in the mineral are exchanged for protons of sulfuric acids. The $Na^+$ cations were the most removed cations, because these elements were present in the interlayer space and displaced by protons easily, while $Mg^{2+}$, $Fe^{3+}$ and $Al^{3+}$ are settled in the octahedral layers which were dissolved with quite difficulty [60-62]. At the same time, the decreases in the contents of $Al_2O_3$ and $Fe_2O_3$ and the increase in the content of $SiO_2$ suggest that $Al^{3+}$ and $Fe^{3+}$ ions leave the alumino-silicates tetrahedral and are displaced by protons of the acid, resulting in an additional number of hydroxyl groups [63]. The reduction in the octahedral cations and increase in the silica content after activation could be as a result of the octahedral sheet destruction passing the cations into the solution, while the silica generated by the tetrahedral sheet remains in the solid state due to insolubility [41]. These reactions lead to a partial destruction of the primary structure of the clay mineral, and, hence, to a

change in their performance [63].

### *B. Column adsorption studies*

#### *1) Effect of initial methylene blue ion concentration*

The effect of initial MB concentration on the breakthrough curve was studied with initial concentrations of 20 mg/L, 50 mg/L, 80 mg/L, and 120 mg/L, at a bed height of 5 cm and flow rate of 0.6 L/min. The results are presented in Figure 5. From the figure, it can be seen that the clay adsorbent gets saturated early at higher inlet concentration thereby reducing the breakthrough time considerably from 15 h (900 min) for 20 mg/L to 4 h (240 min) for 120 mg/L. This can be explained by the fact that at higher initial MB concentration, concentration gradient resulted to a faster transport of the MB molecules due to increased diffusion coefficient/mass transfer coefficients [64]. Also, a higher concentration of MB ions has been shown to lead to a higher driving force for MB ions to overcome the mass transfer resistance in the liquid phase [65].

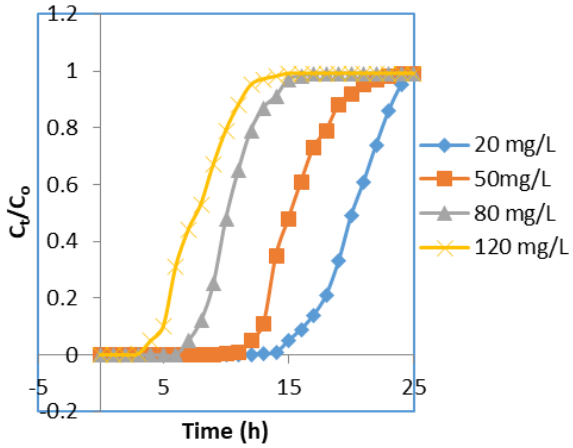


Fig. 5. Breakthrough curves obtained at different initial MB concentrations (flow rate = 0.6 L/min; bed height = 5 cm)

#### *2) Effect of flowrate on the breakthrough curve*

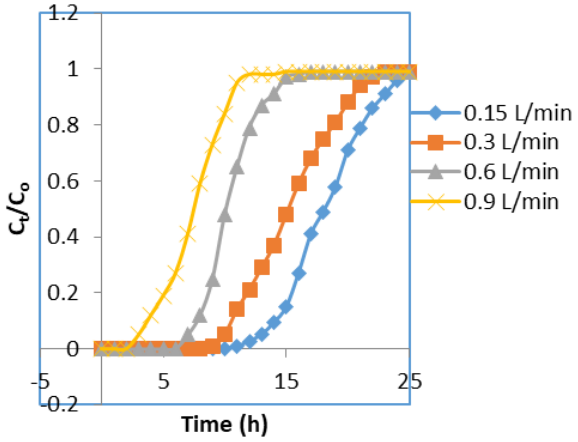


Fig. 6. Breakthrough curves obtained at different inlet flowrates (initial MB concentration = 50 mg/L; bed height = 5 cm)

The effect of inlet flow rate was studied at four different flow rates of 0.15 L/min, 0.30 L/min, 0.6 L/min, and 0.9 L/min at initial MB concentration of 50 mg/L and bed height of 5 cm. The results are shown in Figure 6. From the figure, it can be observed that there was a rapid uptake of dye ions at initial stages, but later on the uptake rate decreased slowly and finally reached equilibrium. Also, the figure shows that the rate of reaching the breakthrough time is faster at higher flow rate whereas the breakthrough time is slower at lower flow rate. This may be due to the residence time distribution of influent concentration to the adsorbent is greater in lower flow rate (11, 65 - 66). As the flow rate increased from 0.15 L/min to 0.9 L/min, the breakthrough time, $t_b$, decreased from 12 h (720 min) to 3 h (180 min). The exhaustion time, $t_e$, decreased from 25 h (1500 min) to 12 h (720 min) as the flow rate increased from 0.15 L/min to 0.9 L/min and this could be attributed to decrease in residence time of adsorbate and external mass transfer resistance at the surface of the adsorbent [11], [48].

#### *3) Effect of bed height on the breakthrough curve*

The effect of bed height on the breakthrough curve of MB adsorption onto modified clay was studied at four different bed heights of 2 cm, 5 cm, 7 cm, and 9 cm, at initial MB concentration of 50 mg/L and influent flow rate of 0.6 L/min, and the results are shown in Figure 7. The figure shows that as the bed height (adsorbent mass) increases, MB molecules had more time to contact the clay adsorbent that resulted in higher removal efficiency in the column. Also, with increase in bed height, the exhaustion time increased from 11 h (660 min) to 23 h (1380 min) as a result of more contact time and availability of more number of surface sites and increased volume influent [48], [67]-[70]. It can also be deduced from the figure that as the bed height increased from 3 cm to 9 cm, the breakthrough time increased from 3 h (180 min) to 11 h (660 min).

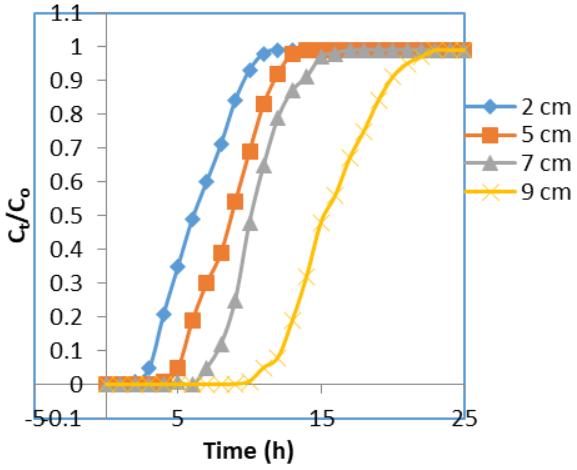


Fig. 7. Breakthrough curves obtained at different bed height (initial MB concentration = 50 mg/L; influent flowrate = 0.6L/min)

### *C. Evaluation of basic design parameters of adsorption column*

The adsorption data for MB uptake in a fixed-bed column were evaluated with respect to the influent MB concentration, flow rate and bed height and are presented in Table 2. The values of the experimental breakthrough parameters summarized in Table 2 indicated that the breakthrough time, $t_b$; exhaustion time, $t_e$; breakthrough effluent volume, $V_B$; and exhaustion effluent volume, $V_E$; were inversely related with influent MB concentration. Also, the MTZ height was longer at

higher initial MB concentrations. This is in agreement with the reports of other researchers [71], [72]. Sorption capacity was observed to increase with increase in initial MB concentration and this could be explained by the fact that at higher concentration, gradient caused a faster transport due to an increased diffusion coefficient or mass transfer coefficient [73]. From Table II, as the flow rate increased from 0.15 to 0.9 L/min, the exhaustion time decreased from 1440 to 660 min, while the mass transfer height, rate, and time increased. Also, the uptake capacity of the column and the removal efficiency increased with increase in flow rate. The decrease in exhaustion time with increase in flow rate could be attributed to decrease in residence time of adsorbate and external mass transfer resistance at the surface of the adsorbent [11], [48]. The table shows that increase in bed height resulted to increase in exhaustion time and influent volume and this is due to the availability of more contact time. Similarly, the removal efficiency, *R*, increased from 89 to 98% with increase in bed height. The increase in efficiency at higher bed height could be due to the availability of more number of surface sites and increased influent volume [67].

### *D. Breakthrough curve modeling*

The breakthrough curves obtained for initial methylene blue ion concentration, flow rate, and bed height can well be explained by simple mathematical models. These breakthrough curves were then predicted with well-known mathematical models such as Thomas, Adams-Bohart, and Yoon-Nelson models.

#### *1) Thomas model*

The Thomas model (74) is one of the most widely used mathematical models in column performance analysis. The linearized form of this model can be expressed in equation (12) [75],

$$\ln\left(\frac{C_0}{C_t} - 1\right) = \frac{k_{Th} q_e W}{Q} - k_{Th} C_0 t \quad (12)$$

Where $k_{Th}$ is the Thomas rate constant (L/min.mg), $q_e$ is the equilibrium adsorption of MB (mg/g), $C_0$ is the inlet MB concentration (mg/L), $C_t$ is the effluent MB concentration at time $t$ (mg/L), $W$ is the mass of adsorbent in the column (g), $Q$ is the inlet flow rate (L/min), and $t$ is the flow time (min). The kinetic coefficient $k_{Th}$ and the adsorption capacity of the column $q_e$ can be determined from linear plot of $ln\ (C_0/C_t - 1)$ against $t$ for a given initial concentration, flow rate or bed height.

The obtained column data were fitted to the Thomas model to determine the Thomas rate constant $(k_{Th})$ and equilibrium adsorption capacity $(q_e)$. The values of $k_{Th}$ and $q_e$ obtained for all the breakthrough curves together with the correlation coefficients are presented in Table 3. It can be observed from Table 3 that as initial MB concentration increases from 20 to

Table 2
Column data and parameters obtained under different operating conditions

| Column parameter | | Column performance variables | | | | | | | | | | |
|---|---|---|---|---|---|---|---|---|---|---|---|---|
| | | $t_b$ (min) | $t_e$ (min) | $V_B$ (L) | $V_E$ (L) | $t_z$ (min) | $U_z$ (cm/min) | $h_z$ (cm) | $q_{total}$ (mg) | $q_{exp}$ (mg/g) | $W_{total}$ (mg) | R (%) |
| Initial MB concentration (mg/L) | 20 | 900 | 1440 | 540 | 864 | 540 | 0.0035 | 1.875 | 15.552 | 17.28 | 17.28 | 90 |
| | 50 | 720 | 1260 | 432 | 756 | 540 | 0.0040 | 2.143 | 35.721 | 39.69 | 37.80 | 95 |
| | 80 | 420 | 840 | 252 | 540 | 480 | 0.0060 | 2.500 | 39.603 | 44.00 | 43.20 | 92 |
| | 120 | 240 | 720 | 144 | 432 | 480 | 0.0069 | 3.333 | 46.656 | 51.84 | 51.84 | 90 |
| Flow rate (L/min) | 0.15 | 780 | 1440 | 117 | 216 | 660 | 0.0035 | 2.292 | 9.78 | 10.87 | 10.80 | 91 |
| | 0.3 | 600 | 1260 | 180 | 378 | 660 | 0.0040 | 2.619 | 17.62 | 19.58 | 18.90 | 93 |
| | 0.6 | 420 | 900 | 252 | 540 | 480 | 0.0056 | 2.667 | 25.93 | 28.81 | 27.00 | 96 |
| | 0.9 | 180 | 660 | 162 | 594 | 480 | 0.0076 | 3.636 | 28.87 | 32.08 | 29.70 | 97 |
| Bed height (cm) | 2 | 180 | 630 | 108 | 378 | 450 | 0.0032 | 1.429 | 16.79 | 20.98 | 18.90 | 89 |
| | 5 | 300 | 750 | 180 | 450 | 450 | 0.0067 | 3.000 | 20.88 | 22.38 | 22.50 | 93 |
| | 7 | 420 | 870 | 252 | 522 | 450 | 0.0080 | 3.621 | 25.06 | 23.29 | 26.10 | 96 |
| | 9 | 660 | 1260 | 396 | 756 | 600 | 0.0071 | 4.286 | 36.97 | 24.65 | 37.80 | 98 |

Table 3
Thomas, Adams-Bohart, and Yoon-Nelson models parameters at different experimental conditions

| Models | Constants | Column Parameters | | | | | | | | | | | |
|---|---|---|---|---|---|---|---|---|---|---|---|---|---|
| | | Initial concentration (mg/L) | | | | Flow rate (L/min) | | | | Bed height (cm) | | | |
| | | 20 | 50 | 80 | 120 | 0.15 | 0.3 | 0.6 | 0.9 | 2 | 5 | 7 | 9 |
| Thomas model | $k_{Th}$ x $10^{-3}$ (L/mg.min) | 41.7 | 14.52 | 7.11 | 3.26 | 13.58 | 13.10 | 11.38 | 6.81 | 6.80 | 7.98 | 10.26 | 12.98 |
| | $q_e$ (mg/g) | 37.52 | 78.96 | 92.02 | 95.97 | 21.75 | 38.11 | 57.52 | 64.71 | 66.07 | 39.50 | 38.83 | 32.65 |
| | $R^2$ | 0.9896 | 0.9817 | 0.9694 | 0.9642 | 0.9645 | 0.9327 | 0.9698 | 0.9777 | 0.9274 | 0.9553 | 0.9354 | 0.9461 |
| Adams-Bohart model | $k_{AB}$ x $10^{-3}$ (L/mg.min) | 29.35 | 8.56 | 3.36 | 1.09 | 1.78 | 5.38 | 7.96 | 8.94 | 6.42 | 4.28 | 2.56 | 2.08 |
| | $N_0$ (mg/L) | 53.73 | 125.33 | 185.71 | 271.82 | 32.55 | 61.42 | 115.99 | 171.91 | 277.53 | 115.08 | 83.51 | 70.55 |
| | $R^2$ | 0.8339 | 0.7238 | 0.4632 | 0.4563 | 0.7774 | 0.7023 | 0.4631 | 0.5571 | 0.4293 | 0.5092 | 0.4835 | 0.4667 |
| Yoon-Nelson model | $k_{YN}$ x $10^{-1}$ (L/min) | 8.34 | 7.29 | 5.69 | 3.91 | 6.79 | 6.55 | 5.69 | 3.40 | 3.40 | 3.99 | 5.13 | 6.49 |
| | τ (min) | 20.01 | 16.83 | 12.27 | 8.09 | 18.56 | 16.26 | 12.27 | 6.30 | 5.64 | 8.43 | 11.60 | 16.38 |
| | $R^2$ | 0.9896 | 0.9628 | 0.9697 | 0.8949 | 0.9467 | 0.9328 | 0.8695 | 0.8977 | 0.8875 | 0.8759 | 0.9746 | 0.9868 |

120 mg/L, the values of $k_{Th}$ decreased from 0.0417 to 0.0033 L/min.mg, while $q_e$ increased from 37.52 to 95.97 mg/g. This observation could be attributed to the driving force for adsorption as a result of the concentration difference between the dye molecules on the adsorbent and the dye molecules in the solution. Thus, the high driving force due to the higher MB concentration resulted to a better column performance [11], [76]-[77]. Similar observation was reported by other researchers [48], [78]-[79]. The values of equilibrium adsorption capacity, $q_e$, changed significantly with increased flow rate. As flow rate increased from 0.15 to 0.9 L/min, $q_e$ increased from 21.75 to 64.71 mg/g, similar to the findings of others [11], [17], [66], [80]-[81]. On the other hand, the values of $k_{Th}$ and $q_e$ decreased as the flow rate and bed height increased, respectively. The $R^2$ values for the Thomas model plots were in the range of 0.9276 to 0.9897 which shows that this model fits well with the experimental data and could be used to predict that the MB adsorption on activated Kono-bowe clay is a monolayer adsorption.

*2) Adams-Bohart model*

Adams-Bohart model [82] is usually used to explain the initial part of the breakthrough curve and it assumes that equilibrium is not instantaneous and the rate of sorption is proportional to the fraction of sorption capacity [48,83]. The model equation is expressed in linear form as shown in equation (13):

$$\ln\left(\frac{C_t}{C_0}\right) = k_{AB}C_0 t - k_{AB}N_0\left(\frac{z}{U_0}\right) \quad (13)$$

Where $C_0$ and $C_t$ are the inlet and outlet MB concentrations (mg/L), $k_{AB}$ is the kinetic constant (L/mg.min), $N_0$ is the saturation concentration (mg/L), Z is the bed height (cm), and $U_0$ is superficial velocity (cm/min). To estimate the values of the model parameters, values of $ln\ (C_t/C_0)$ were plotted against t (time) and $k_{AB}$ and $N_0$ were calculated from the slope and intercept of the linear regression, respectively. The calculated values are presented in Table 3. From Table 3, it could be observed that the values of $k_{AB}$ decreased with increase in initial MB ion concentration and increase in bed height but increased with increase in flow rate. The same trend was reported in the literature [48], [84]. $N_0$ values were found to increase with increase in initial MB concentration and increase in bed height, while it decreased with increase in flow rate. From Table III it is obvious that this model does not fit into the experimental data for the values of the coefficient of determination $R^2$ show distribution between 0.4293 and 0.8339.

*3) Yoon-Nelson model*

This model assumes that the rate of decrease in the adsorption probability for each adsorbate molecules is proportional to the sorbate sorption probability and sorbate breakthrough on sorbent [48], [85]. This model is not only less complicated than other models, but also requires no detailed data concerning the characteristics of adsorbate, type of adsorbent, and the physical properties of the adsorption bed [11], [77]. The linear form of the Yoon-Nelson model is shown in equation (14):

$$\ln\left(\frac{C_t}{C_0 - C_t}\right) = k_{YN}t - \tau k_{YN} \quad (14)$$

Where $k_{YN}$ is the Yoon-Nelson proportionality constant ($min^{-1}$) and τ is the time required for retaining 50% of the initial sorbate (min). The values of $k_{YN}$ and τ were determined from the slope and intercept of the plot of $ln\ (C_t/C_0 - C_t)$ versus $t$ and are presented in Table 3. From the table, the values of $k_{YN}$ decreased with increase in initial MB concentration and increase in flow rate, but it increased with increase in the bed height. This is in agreement with the findings of Chowdhury et al. (84) and Lakshmipathy and Sarada [48]. The values of τ, time necessary to reach 50% retention, was found to significantly decrease with increase in initial MB concentration and increase in flow rate. This could be as a result of quick column saturation attained as the parameters increase. The τ values increased with increase in bed height as a result of slower saturation of column bed at higher bed heights. The regression coefficients obtained from this model plots ranges from 0.8695 to 0.9896 and this shows that the model fits the experimental data and can be employed in the prediction of MB adsorption on activated clay in a column mode.

*E. Bed depth service time (BDST)*

The bed depth service time model is used to predict the relationship between bed depth and service time, in terms of adsorption process parameters. It is based on the assumption that the rate of adsorption is controlled by surface reaction between adsorbate and the unused capacity of the adsorbent [86], [87]. The linear relationship between the bed depth, $Z$, and the service time at breakthrough, $t_B$, is given in equation (15);

$$t_B = \frac{N_0}{C_0 Q}Z - \frac{1}{K_a C_0}\ln\left(\frac{C_0}{C_t} - 1\right) \quad (15)$$

Where $N_0$ is the column adsorption capacity in BDST model (mg/L), $Q$ is the flow rate (L/min), and $K_a$ is the adsorption rate constant (L/mg.min). The values of $N_0$ and $K_a$ were evaluated from the slope and intercept of the linear plot of $t_B$ versus $Z$ and the values are presented in Table 4.

A simplified form of the BDST model is,

$$t_B = aZ - b \quad (16)$$

Where

$$a = \frac{N_0'}{C_0 Q} \quad (17)$$

$$b = \frac{1}{K_a C_0}\ln\left(\frac{C_0}{C_t} - 1\right) \quad (18)$$

The slope constant for other flow rates and influent concentrations can be calculated directly by equations (19) and (20), respectively [87].

$$a' = a\frac{Q}{Q'} \quad (19)$$

Table 4
Calculated constants of BDST model for the adsorption of MB onto modified Kono-bowe clay using linear regression

| $C_t/C_o$ | Model constants | | | | | | | | |
|---|---|---|---|---|---|---|---|---|---|
| | $C_o$ (mg/L) | $C_o'$ (mg/L) | a (min/cm) | a' (min/cm) | b (min) | b' (min) | $N_o$ (mg/L) | $K_a$ (L/mg.min) | $R^2$ |
| 0.05 | | 20 | | 0.354 | | 0.497 | 4.248 | 0.2962212 | |
| | 50 | | 0.885 | | 0.634 | | 26.55 | 0.0928852 | 0.9985 |
| | | 80 | | 1.416 | | 1.163 | 67.97 | 0.0316470 | |
| | | 120 | | 2.124 | | 1.842 | 152.93 | 0.0133208 | |
| 0.10 | | 20 | | 0.380 | | 0.516 | 4.56 | 0.2129094 | |
| | 50 | | 0.950 | | 2.209 | | 28.50 | 0.0198933 | 0.9978 |
| | | 80 | | 1.520 | | 2.834 | 72.96 | 0.0096914 | |
| | | 120 | | 2.280 | | 3.679 | 164.16 | 0.0049800 | |
| 0.40 | | 20 | | 0.4008 | | 2.391 | 4.81 | 0.0084789 | |
| | 50 | | 1.002 | | 4.625 | | 30.06 | 0.0017532 | 0.9997 |
| | | 80 | | 1.6032 | | 5.928 | 76.95 | 0.0008550 | |
| | | 120 | | 2.4048 | | 7.853 | 173.15 | 0.0004303 | |
| 0.80 | | 20 | | 0.4712 | | 4.694 | 5.65 | -0.014766 | |
| | 50 | | 1.178 | | 7.168 | | 35.34 | -0.003868 | 0.9989 |
| | | 80 | | 1.8848 | | 9.852 | 90.47 | -0.001758 | |
| | | 120 | | 2.8272 | | 11.65 | 203.56 | -0.000992 | |

$$a' = a\frac{C_0}{C_0'} \tag{20}$$

Where *a, Q*, and $C_0$ are the old slope, influent flow rate, and inlet MB concentration and *a', Q'*, and $C_0'$ are the new slope, influent flow rate and inlet MB concentration, respectively. A new intercept is given by equation (21) [66].

$$b' = b\frac{C_0}{C_0'}\left(\frac{ln(C_0'-1)}{\ln(C_0-1)}\right) \tag{21}$$

Where *b'* and *b* are the new and old intercept, respectively.

The plots of *t* versus bed depth, *Z*, at $C_t/C_0$ values of 0.05, 0.1, 0.4, and 0.8 are shown in Figure 8.

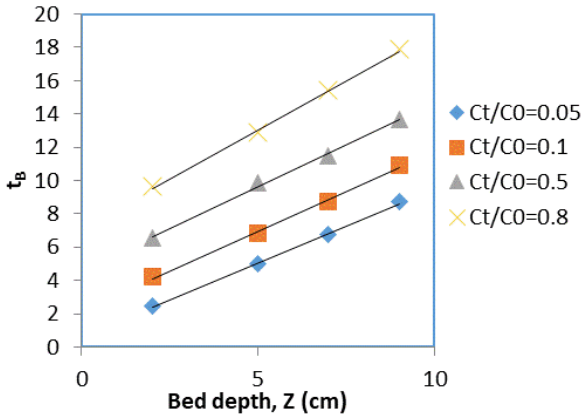


Fig. 8. Bed depth service time of column at different bed height (Co = 50 mg/L and Q = 0.6 L/min)

The calculated values of the related constants are listed in Table 4. Also, the predicted constants for other process parameters were scaled up from the values at $C_0$ = 50 mg/L, *Q* = 0.6 L/min and are listed in Table 4 alongside other values. From Table 4, it was observed that the values of the adsorption capacity, $N_0$, increased with increase in the value of $C_t/C_0$, while the rate constant decreased. From the values of coefficient of determination, $R^2$, obtained from the plots, ranging from 0.9972 to 0.9998, it indicated the validity of the BDST model to explain the column performance during MB adsorption onto activated Kono-bowe clay. Similar observation was recorded by other researchers [66], [88].

## 4. Conclusion

Modified Kono-bowe clay was used as an adsorbent for methylene blue adsorption from aqueous solution in a fixed-bed column. The acid activation of the natural clay and subsequent calcination at 450 $^0$C improved the performance of the clay by increasing the surface area, cation exchange capacity and sorption performance. The column studies were performed by varying initial MB concentration, flow rate, and bed height and the adsorption of MB onto modified Kono-bowe clay was observed to be a function of these column parameters. The breakthrough and exhaustion times were observed to decrease with increase in initial MB concentration and increase in flow rate but increases with increase in bed height. The study of the variation of the mass transfer zone (MTZ) at different operating conditions shows that the rate and height of the mass transfer region increases with increase in initial MB concentration, flow rate, and bed height. The experimental data showed a better fit to the Thomas and Yoon-Nelson adsorption models proving that these models can be used to describe the behavior of adsorption of MB onto modified clay sorbent in a continuous fixed-bed column.

## Declaration of competing interest

The authors declare that they have no known competing financial interests or personal relationships that could have appeared to influence the work reported in this paper.

## References

[1] Sokolowska, G. (1996). Synthetic dyes based on environmental considerations, *Dye pigment*, 30(1): 1-18.

[2] Ivanov, K. (1996). Possibilities of using zeolite as filler and carrier for dyestuffs in paper. *Papier-Zeitschrift fur die erzeugung von holzstoff zellstoff papier und pappe*, 50(7): 456-469.

[3] Kabdasli, I., Tunay, O. and Orhon, D. (1996). Wastewater control and management in a leather tanning district. *Water Sci. Technol*., 40(1): 261-277.

[4] Bensalah, N., Alfaro, M. and Martinez-Huitle, C. (2009). Electrochemical treatment of synthetic wastewaters containing alphazurine A dye. *Chem. Eng. J.*, 149(1): 348-359.

[5] Wrobel, D., Boguta, A. and Ion, R.M. (2001). Mixtures of synthetic organic dyes in a photoelectrochemical cell. *J. Photochem. Photobio. A: Chem*., 138(1): 7-14.

[6] Dawood, S., Sen, T.K. and Phan, C. (2014). Synthesis and characterization of novel-activated carbon from waste biomass pine cone and its application in the removal of Congo red dye from aqueous solution by adsorption. *Water, Air, Soil Poll.*, 225(1): 1-13.

[7] Yagub, M.T., Sen, K.T., Afroze, S. and Ang, H.M. (2014). Dye and its removal from aqueous solution by adsorption: a review. *Advances Colloid Interface Sci.*, 209: 172-186.

[8] Sen, T.K., Afronze, S. and Ang, H.M. (2011). Equilibrium, kinetics and mechanism of removal of methylene blue from aqueous solution by adsorption onto pine cone biomass of pinus radiate. *Water, Air, Soil Poll.*, 218: 499-508.

[9] Yagub, M.T., Sen, T.K. and Ang, H.M. (2012). Equilibrium, kinetics, and thermodynamics of methylene blue adsorption by pine tree leaves. *Water, Air, Soil Poll.*, 223(8): 5267-5275.

[10] Rehman, M.S.U., Kim, I., Han, J.I. (2012). Adsorption of methylene blue dye from aqueous solution by sugar extracted spent rice biomass. *Carbohydrate Poly*., 90(3): 1314-1326.

[11] Han, R., Wang, Y., Zhao, X., Wang, Y., Xie, F., Cheng, J. and Tang, M. (2009a). Adsorption of methylene blue by phoenix tree leaf powder in a fixed-bed column: Experiments and prediction of breakthrough curves. *Desalination*: 245: 284-296.

[12] Vadivelan, V. and Kumar, K.V. (2005). Equilibrium, kinetics, Mechanism, and process design for the sorption of methylene blue onto rice husk. *J. Colloid Interface Sci.*, 286(1): 90-101.

[13] Raghu, S. and Basha, C.A. (2007). Chemical or electrochemical techniques, followed by ion exchange for recycle of textile dye wastewater. *J. Hazard Mater.*, 149(2): 324-331.

[14] Bastaki, N. (2004). Removal of methyl orange dye and $Na_2SO_4$ salt from synthetic wastewater using reverse osmosis. *Chem. Eng. Process*, 43(12): 1561-1574.

[15] Purkait, M.K., Gupta, S.D. and De, S. (2006). Performance of TX-100 and TX-114 for the separation of chrysoidine dye using cloud point extraction. *J. Hazard Mater.*, 137(2): 827-835.

[16] Huang, Y.H., Huang, Y.F., Chang, P.S. and Chen, C.Y. (2008). Comparative study of oxidation of dye-reactive black B by different advanced oxidation processes: Fenton, electro-fenton and photo-fenton, *J. Hazard. Mater.*, 154(1-3): 655-662.

[17] Hasfalina, C.B., Akinbile, C.O. and Jun, C.X. (2015). Coconut husk adsorbent for the removal of methylene blue dye from wastewater. *Bioresources*, 10(2): 2859-2867.

[18] Baral, S.S., Das, S.N., Chaudhury, G.R., Swamy, Y.V. and Rath, P. (2008). Adsorption of Cr (VI) using thermally activated weed salninia cucullate. *Chem. Eng. J.*, 139: 245-253.

[19] Yagub, M.T., Sen, T.K. and Ang, M. (2013). Removal of cationic dye methylene blue (MB) from aqueous solution by ground raw and base modified pine cone powder Environ. *Earth Sci*., 13: 1-13.

[20] Dawood, S. and Sen, T.K. (2012). Removal of anionic dye Congo red from aqueous solution by raw pine and acid-treated pine cone powder as adsorbent: equilibrium, thermodynamic, kinetics, mechanism and process design. *Water Res*., 46(6): 1933-1942.

[21] Ghosh, R.K. and Reddy, D.D. (2013). Tobacco stem ash as an adsorbent for removal of methylene blue from aqueous solution: equilibrium, kinetics, and mechanism of adsorption. Water, *Air Soil Poll.*, 224(6): 1-15.

[22] Zhang, J., Zhou, Q. and Ou, I. (2012). Kinetic, isotherm, and thermodynamic studies of the adsorption of methyl orange from aqueous solution by chitosan/alumina composite, *J. Chem. Eng. Data,* 67: 412-423.

[23] Sanghi, R. and Verma, P. (2013). Decolorisation of aqueous dye solutions by low-cost adsorbents: A review. *Colour Technol.*, 129: 1-10.

[24] Srivastava, P., Goyal, S. and Tayade, R. (2013). Ultrasound-assisted adsorption of reactive blue 21 dye on $TiO_2$ in the presence of some rare earths (La, Ce, Pr and Gd). Cana. *J. Chem. Eng*., 99: 1-12.

[25] Han, X., Niu, X. and Ma, X. (2012). Adsorption characteristics of methylene blue on poplar leaf in batch mode: equilibrium, kinetics and thermodynamics, Korean J. Chem. Eng., 1-9, 2012.

[26] Bello, O.S. and Ahmad, M.A. (2012). Coconut (cocos nucifera) shell based activated carbon for the removal of malachite green dye from aqueous solutions, *Sep. Sci. Technol.*, 47(6): 903-909.

[27] Chowdhury, A.K., Sarkar, A.D. and Bandyopadhyay, A. (2009). Rice husk ash as a low-cost adsorbent for the removal of methylene blue and Congo red in aqueous phases. *Clean*, 37(7): 581-590.

[28] El Qada, E.N., Allen, S.J. and Walker, G.M. (2008). Adsorption of basic dyes from aqueous solution onto activated carbons, *Chem. Eng J.*, 135: 174-186.

[29] Kumar, P., Ramalingam, S. and Sathishkumar, K. (2011). Removal of methylene blue dye from aqueous solution by activated carbon prepared from cashew nut shell as a new low-cost adsorbet. *Korean J. Chem. Eng.*, 28: 149-161.

[30] Karaca, S., Gürses, A., Açıkyıldız, M. and Ejder, M. (2008). Adsorption of cationic dye from aqueous solutions by activated carbon, *Micropor Mesopor Mat*., 115: 376-384.

[31] Liu, P. and Zhang, L. (2007). Adsorption of dyes from aqueous solutions or suspensions with clay nano adsorbents. *Sep. Purif Technol*., 58: 32-43.

[32] Nandi, B.K., Goswami, A. and Purkait, M.K. (2009a). Adsorption characteristics of brilliant green dye on kaolin. *J. Hazard Mater.*, 161: 387-396.

[33] Gürses, A., Doğar, C., Yalçın, M., Açıkyıldız, M., Bayrak, R. and Karaca, S. (2006). The adsorption kinetics of the cationic dye, methylene blue, onto clay. *J Hazard Mater*., 131: 217-228.

[34] Wang, S., Li, H. and Xu, L. (2006). Application of zeolite MCM-22 for basic dye removal from wastewater. *J. Colloid Interf Sci.*, 295: 71-79.

[35] McKay, G. (1984). The Adsorption of basic dye onto silica from aqueous solution-solid diffusion model. *Chem. Eng. Sci.*, 39: 129-137.

[36] Tang, H., Zhou, W. and Zhang, L. (2012). Adsorption isotherms and kinetics studies of malachite green on chitin hydrogels. *J. Hazard Mater.*, 209–210: 218-229.

[37] Dotto, G.L., Vieira, M.L.G. and Pinto, L.A.A. (2012). Kinetics and mechanism of tartrazine adsorption onto chitin and chitosan. *Ind. Eng. Chem. Res.*, 51: 6862-6875.

[38] El Qada, E.N., Allen, S.J. and Walker, G.M. (2007). Kinetic modeling of the adsorption of basic dyes onto steam-activated bituminous coal. *Ind Eng Chem. Res*. 46: 4764-4774.

[39] DeSales, P.F., Magriotis, Z.M., Rossi, M.A., Resende, R.F., and Nunes, C.A. (2013). Optimization by response surface methodology of the adsorption of coomassie blue dye on natural and acid-treated clays. *J. Environ. Manag.*, 130: 417-425.

[40] Tanabe, K. *Solid acid and base catalysis: in Catalysis Science and Technology*, in: J. R. Anderson, M. Boudart (Eds.), Springer Verlag, New York 1981.

[41] Ajemba, R.O. (2014). Kinetics and equilibrium modeling of lead (II) and chromium (III) ions' adsorption onto clay from Kono-bowe, Nigeria, *Turkish J. Engr. Environ. Sci.*, 38: 455-480.

[42] Theocharis, C.R., Jacob, K.J. and Gray, A.C. (1988). Enhancement of Lewis acidity in layer aluminosilicates. *J. Chem. Soc. Faraday Trans.*, 84: 1509-1514.

[43] Sarma, G.K., SenGupta, S. and Bhattacharyya, K.G. (2011). Methylene Blue Adsorption on Natural and Modified Clays, *Sep. Sci. Technol.*, 46 (10): 1602-1612.

[44] Suraj, G., Iyer, C.S.P. and Lalithambika, M. (1998). Adsorption of cadmium and copper by modified kaolinite. *Appl. Clay Sci.*, 13: 293-302.

[45] Roulia, M. and Vassiliadis, A.A. (2008). Sorption characterization of a cationic dye retained by clays and perlite, Micro. Meso. Mater., 116: 732-741.

[46] Almeida, C.A.P., Debacher, N.A., Downs, A.J., Cottet, L. and Mello, C.A.D. (2009). Removal of methylene blue from colored effluents by adsorption on montmorillonite clay. *J. Colloid Interface Sci.*, 332: 46-58.

[47] Nandi, B.K., Goswami, A. and Purkait, M.K. (2009b). Removal of cationic dyes from aqueous solutions by kaolin: Kinetic and equilibrium studies, *Appl. Clay Sci.*, 42: 583-595.

[48] Lakshmipathy, R. and Sarada, N.C. (2015). Methylene blue adsorption onto native watermelon rind: batch and fixed bed column studies. *Desalination Water Treat.*, DOI: 10.1080/19443994.2015.1040462.

[49] Espantaleon, A.G., Nieto, J.A., Fernandez, M. and Marsal, A. (2003). Use of activated clays in the removal of dyes and surfactants from tannery waste waters. *Appl. Clay Sci.*, 24: 105-112.

[50] Sears, G.W. (1956). Determination of specific surface area of colloidal silica by titration with sodium hydroxide. *Analytical Chem*., 28:1981-1988.

[51] Bergaya, F. and Vayer, M. (1997). CEC of clays: Measurement by adsorption of a copper ethylendiamine complex, *Appl. Clay Sci.*, 12: 275-281.
[52] Bhattacharyya, K.G. and Gupta, S.S. (2006). Pb (II) uptake by kaolinite and montmorillonite in aqueous medium: influence of acid activation of the clays. *Colloids Surf. A: Physicochem. Eng. Aspects*, 277: 191-201.
[53] Diaz, F.R.V. and Sanctos, P.S. (2001). Studies on the acid activation of Brazilian smectite clays, *Quim. Nova*, 24: 345.
[54] Lopez-Gonzalez, J.D. and Deitz, V.R. (1952) Surface changes in an original and activated bentonite, *J. Res*., 48: 325-333.
[55] Leposava, F. and Perovic, L. (2002). The effects of fine grinding on the physicochemical properties and thermal behavior of bentonite clay. *J. Serb. Chem. Soc.*, 67: 753-764.
[56] Onal, M. (2007). Changes in crystal structure, thermal behavior and surface area of bentonite by acid activation. *Commun. FacSei llniv Ank B*, 53: 1-9.
[57] Foletto, E.L., Volzone, C. and Porto, L.M. (2003) Performance of an Argentinean acid-activated bentonite in the bleaching of soybean oil. *Braz. J. Chem. Eng.*, 20: 213-220.
[58] Giustetto, R., Wahyudi, O., Corazzari, I. and Turci, F. (2011). Chemical stability and dehydration behavior of a sepiolite/indigo maya blue pigment, *Appl. Clay Sci.*, 52: 41-57.
[59] Dikmen, S., Yilmaz, G., Yorukogullari, E., Korkmaz, E. (2012). Zeta potential study of natural- and acid-activated sepiolites in electrolyte solutions, Can. *J. Chem. Eng.*, 90: 785-791.
[60] Kooli, F. and Liu, Y. (2013) Chemical and thermal properties of organoclays derived from highly stable bentonite in sulfuric acid. *Appl. Clay Sci*., 83–84: 349-361.
[61] Kooli, F., Liu, Y., Al-Faze, R. and Al-Suhaimi, A. (2015). Effect of acid activation of Saudi local clay mineral on removal properties of basic blue 41 from an aqueous solution. *Appl. Clay Sci.*, 116–117: 23-34.
[62] Tomić, Z.P., Antić Mladenović, S.B., Babić, B.M., Poharc Logar, V.A., Dorđević, A.R. and Cupać, S.B. (2011). Modification of smectite structure by sulphuric acid and characteristics of the modified smectite. *J. Agric. Sci.*, 56: 25-36.
[63] Novikova, L.A., Bel'chinskaya, L.I. and Roessner, F. (2006). Effect of Treatment with Acids on the State of the Surface of Natural Clay Minerals. *Russian J. Phys. Chem.*, 80(1): S185-S194.
[64] Uddin, M.T., Rukanuzzaman, M., Khan, M.M.R. and Islam, M.A. (2009). Adsorption of methylene blue from aqueous solution by jackfruit (Artocarpus heteropyllus) leaf powder: a fixed-bed column study, *J. Environ. Manag.*, 90(11): 3443-3456.
[65] Sugashini, S. and Sheriffa-Begum, K.M. (2013). Column adsorption studies for the removal of Cr (VI) ions by ethylamine modified chitosan carbonized rice husk composite beads with modeling and optimization. *J. Chem*., 1 – 3. DOI: dx.doi.org/ 10.1155/2013/460971.
[66] Han, R., Wang, Y., Yu, W., Zou, W., J., Shi, J. and Liu, H. (2007). Biosorption of methylene blue from aqueous solution by rice husk in a fixed-bed column, J. Hazard. Mater., 141(3): 713-725.
[67] Baral, S.S., Das, N., Ramulu, T.S., Sahoo, S.K., Das, S.N. and Chaudhury, G.R. (2009) Removal of Cr (VI) by thermally activated weed salvinia cucullata in a fixed-bed column. *J. Hazard Mater*., 161: 1427-1441.
[68] Song, J.Y., Zou, W.H., Bian, Y.Y., Su, F.Y. and Han, R.P. (2011). Adsorption characteristics of methylene blue by peanut husk in batch and column modes. *Desalination*. 265: 119-127.
[69] Auta, M. and Hameed, B.H. (2014). Chitosan-clay composite as highly effective and low-cost adsorbent for batch and fixed-bed adsorption of methylene blue. *Chem. Eng. J.*, 237: 352-364.
[70] Zhang, W., Dong, L., Yan, H., Li, H., Jiang, Z., Kan, X., Yang, H., Li, A. and Cheng, R. (2011). Removal of methylene blue from aqueous solutions by straw-based adsorbent in a fixed-bed column. *Chem. Eng. J*., 173: 429-438.
[71] Long, Y., Lei, D., Ni, J., Ren, Z., Chen, C. and Xu, H. (2014). Packed bed column studies on lead (II) removal from industrial wastewater by modified Agaricus bisporus. *Bioresource Technol*., 152: 457-463.
[72] Cruz-Olivares, J., Perez-Aonso, C., Barrera-Diaz, C., Urena-Nunez, F., Chaparro-Mercado, M.C. and Bilyeu, B. (2013). Modeling of lead (II) biosorption by residue of allspice in a fixed-bed column. *Chem. Eng. J.*, 228: 21-32.
[73] Samuel, J., Pulimi, M., Paul, M.I., Maurya, A., Chandrasekaran, N., Mukherjee, A. (2013). Batch and continuous flow studies of adsorptive removal of Cr (VI) by adapted bacterial consortial immobilized in alginate beads. *Bioresource Technol.*, 128: 423-434.
[74] Thomas, H.C. (1944). Heterogeneous ion exchange in a flowing system. *J. Am. Chem. Soc.,* 66: 1664-1669.
[75] Ahmad, A.A. and Hameed, B.H. (2010). Fixed-bed adsorption of reactive azo dye onto granular activated carbon prepared from waste. *J. Hazard. Mater*, 175 (1-3): 298-309.
[76] Han, R.P., Zhang, J.H., Zou, W.H., Xiao, H.J., Shi, J. and Liu, H.M. (2006). Bio-sorption of copper (II) and lead (II) from aqueous solution by chaff in a fixed-bed column, J. Hazard. Mater., 133: 262-275.
[77] Aksu, Z. and Gonen, F. (2004). Biosorption of phenol by immobilized activated sludge in a continuous packed bed; prediction of breakthrough curves, *Process Biochem*., 39: 599-607.
[78] Nur, T., Loganathan, P., Nguyen, T.C., Vigneswaran, S., Singh, G. and Kandasamy, J. (2014). Batch and column adsorption and desorption of fluoride using hydrous ferric oxide: solution chemistry and modeling. *Chem. Eng. J.*, 247: 93-102.
[79] Ghribi, A. and Chlendi, M. (2011). Modeling of fixed bed adsorption: application to the adsorption of an organic dye. *Asian J. Chem*., 1(4): 161-172.
[80] Padmesh, T.V.N., Vijayaraghavan, K., Sekaran, G. and Velan, M. (2005). Batch and column studies on biosorption of acid dyes on fresh water macro alga Aolla filiculoides. *J. Hazard Mater*., 125(1-3): 121-135.
[81] Oladoja, N., Aboluwoye, C., Oladimeji, Y. and Otemuyiwa, I. (2008). Studies on castor seed shell as a sorbent in basic dye contaminated wastewater remediation, Desalination, 227(1-3): 190-203.
[82] E.Q. Adams, E.Q., G.S. Bohart, G.S. (1920). Behavior of charcoal towards chlorine. *J. Am. Chem. Society*, 42: 523-538.
[83] Lehmann, M., Zouboulis, A.I. and Matis, K.A. (2001). Modeling the sorption of metals from aqueous solutions on goethite fixed-beds. *Environ. Poll*., 113: 121-133.
[84] Chowdhury, Z.Z., Zain, S.M., Rashid, A.K., Rafique, R.F. and Khalid, K. (2013). Breakthrough curve analysis for column dynamics sorption of Mn(II) ions from wastewater by using mangostana garcinia peel-based granular-activated carbon. *J. Chem.*, 2013: 1 – 8.
[85] Yoon, Y.H. and Nelson, J.H. (1984). Application of gas adsorption kinetics I: A theoretical model for respirator catridge service life. *Am. Ind. Hyg. Assoc. J*., 45: 509-523.
[86] Han, R.P., Zou, L.N., Zhao, X., Xu, Y.F., Xu, F., Li, Y.L. and Wang, Y. (2009b). Characterization and properties of iron oxide-coated zeolite as adsorbent for removal of copper (II) from solution in fixed bed column. *Chem. Eng. J.*, 149: 123-139.
[87] Goel, J., Kadirvelu, K., Rajagopal, C., and Garg, V.K. (2005). Removal of lead (II) by adsorption using treated granular activated carbon; batch and column studies, J. Hazard. Mater., 125: 211-224.
[88] Albadarin, A.B., Mangwandi, C., Al-Muhtaseb, A.H., Walker, G.M., Allen, S.J. and Ahmad, M.N.M. (2012). Modeling and fixed-bed column adsorption of Cr(VI) onto ortho-phosphoric acid-activated lignin. *Chin. J. Chem. Eng.*, 20(3): 469-478.